

Spontaneous symmetry breaking in two dimensions under nonequilibrium laminar flows

Yuki Minami

*Faculty of Engineering, Gifu University,
1-1 Yanagido, Gifu 501-1193, Japan*

Hiroyoshi Nakano

Institute for Solid State Physics, University of Tokyo, Kashiwa, Chiba 277-8581, Japan

(Dated: August 23, 2024)

Abstract

We study the long-range order in two dimensions where an order parameter is advected by laminar flows such as rotational, shear, and elongational flows. Under these flows, we analyze an ordered state of the $O(N)$ scalar model in the large- N limit. We show that the stability of the ordered state depends on the flow pattern; shear and elongational flows stabilize the long-range order but rotational flow does not. We discuss the physical mechanism underlying our results by connecting static correlations of fluctuations and their dynamics based on the interaction representation used in quantum mechanics. We find that advective transport induces superdiffusion under shear and elongational flows, thereby stabilizing the long-range order.

I. INTRODUCTION

The Hohenberg–Mermin–Wagner (HMW) theorem, a cornerstone of equilibrium statistical mechanics, states that the long-range order (LRO) associated with the spontaneous breaking of continuous symmetry is prohibited below two dimensions (2D) [1, 2]. This theorem is applicable to various equilibrium systems, including ferromagnets [2, 3], crystalline solids [4, 5], and equilibrium flocking models [6]. However, proofs of the HMW theorem are valid only for systems in thermal equilibrium, leaving open the possibility of LRO under nonequilibrium conditions. Indeed, several examples of nonequilibrium systems that violate the HMW theorem have been reported: the flocking model represented by the Vicsek model [7–20], the sheared model [21–28], the multitemperature conserved model [29–31], the nonreciprocal model [32, 33], the center-of-mass conserving model [34–36], athermal chiral active particles [37, 38], and others [39]. The extension of the HMW theorem to nonequilibrium systems attracts significant interest in the field of statistical mechanics.

Extending the HMW theorem is challenging owing to the diverse nature of nonequilibrium fluctuations. Generally, the spontaneous breaking of continuous symmetry, whether in equilibrium or nonequilibrium systems, gives rise to gapless fluctuations called the Nambu–Goldstone (NG) mode [40–45]. In low-dimensional systems, the NG mode may cause infrared (IR) divergences that destroy LRO [46, 47]. For example, in equilibrium systems, the NG mode $\pi(\mathbf{k})$ behaves as $\langle \pi(\mathbf{k})\pi(-\mathbf{k}) \rangle \sim 1/k^2$ in wavenumber space. Then, the mean square fluctuation in real space is given by

$$\langle \pi(\mathbf{x})^2 \rangle \sim \int_{2\pi/L}^{2\pi/a} \frac{dk k^{d-1}}{(2\pi)^d} \frac{1}{k^2}, \quad (1)$$

where d is the space dimension, L the system size, and a the microscopic grid width. For $d \leq 2$, the fluctuation diverges in the thermodynamic limit $L \rightarrow \infty$, thereby destroying the LRO. Therefore, understanding the singularity of the NG mode in $\mathbf{k} \rightarrow \mathbf{0}$ is crucial for examining the applicability of the HMW theorem in nonequilibrium systems. However, nonequilibrium fluctuations exhibit much more anomalous and complex behaviors than equilibrium ones, depending on the specific nature of the systems considered. Examples include generic long-range correlations [48–52], the hyperuniformity of density fluctuations [53, 54], giant number fluctuations [13, 55–57], the anomalous suppression of critical fluctuations [58–62] and, NG mode splitting into an infinite number of modes [23]. These anomalous fluctuations

may change the behaviors of the NG mode, complicating the extension of the HMW theorem.

One class of systems that violates the HMW theorem is characterized by nonequilibrium advection. The Vicsek model and its extensions fall into this category [7–20], where self-propelled motion induces the advection. Another notable example is the sheared model [21–28], where externally imposed shear flow advects an order parameter. In both cases, analyses of minimal hydrodynamic models have established the occurrence of LRO in 2D. For the Vicsek model and its extensions, the minimal hydrodynamic model is given by [12, 17–19]:

$$\frac{\partial \mathbf{u}(t, \mathbf{x})}{\partial t} + \lambda \mathbf{u}(t, \mathbf{x}) \cdot \nabla \mathbf{u}(t, \mathbf{x}) = -\frac{\delta F[\mathbf{u}]}{\delta \mathbf{u}} + \mathbf{f}(t, \mathbf{x}), \quad (2)$$

where $\mathbf{u}(t, \mathbf{x})$ is the velocity field and $\mathbf{f}(t, \mathbf{x})$ is the Gaussian white noise mimicking errors, and $F[\mathbf{u}] = (\nabla \mathbf{u})^2/2 - a\mathbf{u}^2/2 + b\mathbf{u}^4/4$ is the free energy promoting the formation of a uniform flocking state with $\mathbf{u} \neq 0$. The term $\lambda(\mathbf{u} \cdot \nabla)\mathbf{u}$ represents the self-advection of \mathbf{u} due to the self-propelled motion of microscopic elements. The uniform flocking state appears whenever $\lambda > 0$, although the robustness and stability of this flocking phase remain debated [16, 17]. Note that experimental observations have confirmed the existence of the two-dimensional flocking state [13, 15]. For the sheared model, the minimal hydrodynamic model is given by [21–28]

$$\frac{\partial \phi(t, \mathbf{x})}{\partial t} + \mathbf{v}(\mathbf{x}) \cdot \nabla \phi(t, \mathbf{x}) = -\frac{\delta F[\phi]}{\delta \phi} + \eta(t, \mathbf{x}), \quad (3)$$

where $\mathbf{v}(\mathbf{x}) = (\dot{\gamma}y, 0)$ is the stationary shear flow, $\phi(t, \mathbf{x})$ is the $O(N)$ scalar field, $\eta(t, \mathbf{x})$ is the thermal noise, and $F[\phi] = (\nabla \phi)^2/2 - a\phi^2/2 + b\phi^4/4$ is the free energy promoting the formation of a spin-aligned state with $\phi \neq 0$. The term $\mathbf{v}(\mathbf{x}) \cdot \nabla \phi(t, \mathbf{x})$ represents the advective transport. Recent studies have shown that this minimal model describes p -atic liquid crystals [26, 27]. Furthermore, theoretical analyses and numerical simulations for $N = 2$ have demonstrated the stability of the LRO in 2D [23, 24, 26, 27].

Despite the clear evidence that the nonequilibrium advection of the form $\mathbf{u} \cdot \nabla \mathbf{u}$ or $\mathbf{v} \cdot \nabla \phi$ can qualitatively change the dynamic behaviors and lead to the LRO in 2D, analyses using scaling theory, renormalization group theory, or numerical simulations directly solving (2) or (3) do not fully reveal how the nonequilibrium advection plays a crucial role in the dynamics of these systems and violates the HMW theorem.

The aim of this study is to elucidate the physical mechanism underlying the emergence of the LRO in 2D due to advective transport, with the ultimate goal of extending the HMW

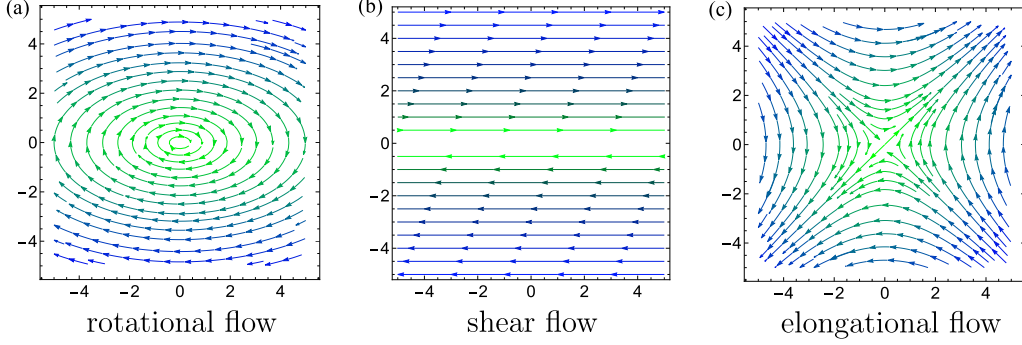


FIG. 1. Three flow patterns of the linear laminar flow (4). (a) Rotational flow at $S = 0.5$ and $A = 1.0$. (b) Shear flow at $S = A = 1.0$. (c) Elongational flow at $S = 1.0$ and $A = 0.0$.

theorem to nonequilibrium systems. For this purpose, we focus on the externally imposed flow and generalize the shear flow to the laminar flow expressed as [63, 64]

$$\mathbf{v}(\mathbf{x}) = \mathcal{D} \cdot \mathbf{x} \quad \text{with} \quad \mathcal{D} = \begin{pmatrix} 0 & S + A \\ S - A & 0 \end{pmatrix}. \quad (4)$$

We call flow (4) the linear laminar flow. Here, \mathcal{D} represents the coefficient matrix, and S and A are non-negative parameters. This stationary flow includes three patterns depending on S and A : rotational flow ($S < A$), shear flow ($S = A$), and elongational flow ($S > A$), the streamlines of which are shown in Fig. 1. Under these various flow patterns, we study the spontaneous symmetry breaking of the $O(N)$ model. We note that phase transitions without symmetry breaking under the linear laminar flow, such as a liquid–gas transition, were previously studied [58, 63, 64].

We demonstrate that in the large- N limit, the shear and elongational flows stabilize the LRO in 2D, whereas the rotational flow does not, which are summarized in Tab. I. This finding implies that nonequilibrium advective transport does not necessarily stabilize LRO in 2D, contrary to findings of the previous studies on the sheared and flocking models. To understand the physical mechanism underlying our results, we connect the static correlation of the NG mode and their dynamics. We apply the interaction representation used in quantum mechanics for decomposing the time evolution of the NG mode by advection and diffusion. In the interaction representation, the advective transport provides the time evolution of the wavenumber along streamlines of the linear laminar flow. We show that the interplay between the advective transport and the diffusive relaxation under the shear and elongational flows leads to the

Type of advection	LRO in 2D	Remarks
Rotational flow	No	New
Shear flow	Yes	Shown in previous studies [23, 24, 26, 27]
Elongational flow	Yes	New
Self-advection	Yes	Not addressed in this paper

TABLE I. Effects of flows on LRO in 2D

superdiffusion of the NG mode, which decays faster than normal diffusion and leads to the LRO in 2D.

II. SETUP

A. Model

We consider a $1 + 2$ dimensional $O(N)$ scalar model subjected to the linear laminar flow (4). Here, the order parameter is given by the N component real scalar field $\phi^a(t, \mathbf{x})$ and its dynamics is described by the nonlinear Langevin equation:

$$\frac{\partial}{\partial t} \phi^a(t, \mathbf{x}) + \mathbf{v}(\mathbf{x}) \cdot \nabla \phi^a(t, \mathbf{x}) = -\Gamma \frac{\delta F}{\delta \phi^a} + \eta^a(t, \mathbf{x}), \quad (5)$$

where $a = 1, 2, \dots, N$, Γ is the dissipation constant, and $\eta^a(t, \mathbf{x})$ is the Gaussian white noise with the temperature T , which obeys

$$\langle \eta^a(t, \mathbf{x}) \eta^b(t', \mathbf{y}) \rangle = 2T\Gamma \delta^{ab} \delta(t - t') \delta(\mathbf{x} - \mathbf{y}). \quad (6)$$

We choose the free energy of the standard form:

$$F = \int d\mathbf{x} \left[\frac{1}{2} \sum_a (\nabla \phi^a)^2 + \frac{r}{2} \sum_a (\phi^a)^2 + \frac{g}{4N} \left(\sum_a (\phi^a)^2 \right)^2 \right]. \quad (7)$$

When the term $\mathbf{v}(\mathbf{x}) \cdot \nabla \phi^a(t, \mathbf{x})$ is absent, our model reduces to the Ginzburg–Landau model [46]. This term gives the advective transport of the order parameter by the flow with the velocity $\mathbf{v}(\mathbf{x})$. When we neglect the right-hand side of (5), it becomes an advection equation, which has the general solution

$$\phi^a(t, \mathbf{x}) = \Phi^a(\mathbf{x} - \mathbf{v}(\mathbf{x})t), \quad (8)$$

for which we have assumed the initial condition $\phi^a(0, \mathbf{x}) = \Phi^a(\mathbf{x})$. This solution means that the order parameter is transported with the velocity $\mathbf{v}(\mathbf{x})$.

Note that our model has the internal $O(N)$ symmetry of ϕ^a . The equation of motion (5) and the noise correlation (6) are covariant under the transformation

$$\phi^a \rightarrow \sum_b [R^n]^a_b \phi_b, \quad \eta^a \rightarrow \sum_b [R^n]^a_b \eta_b, \quad (9)$$

where R^n is the rotation matrix that mixes the internal degrees of freedom a and b . The subscript n specifies the combinations of two components chosen from N components and runs 1, 2..., $N(N-1)/2$. We stress that R^n mixes solely the internal degrees of freedom without mixing the spatial coordinates x and y . Therefore, the advection term $\mathbf{v}(\mathbf{x}) \cdot \nabla \phi^a(t, \mathbf{x})$ does not violate the internal $O(N)$ symmetry, although it explicitly breaks the spatial rotation symmetry.

B. Ordered state at zero temperature

The steady state at $T = 0$ is homogeneous in space and does not depend on the flow $\mathbf{v}(\mathbf{x})$ because the advection term vanishes for homogeneous solutions. The flow effects appear in fluctuations at finite temperatures, as seen in the next section. Then, the steady state is obtained by the minimum of the free energy (7). The saddle point equation is given by

$$\left. \frac{\delta F}{\delta \phi^a} \right|_{\phi^a = \bar{\phi}^a} = \left[r + \frac{g}{N} \sum_b (\bar{\phi}^b)^2 \right] \bar{\phi}^a = 0, \quad (10)$$

which has the disordered solution for $r \geq 0$,

$$\bar{\phi}^a = (0, 0, \dots, 0), \quad (11)$$

and the ordered solution for $r < 0$,

$$\bar{\phi}^a = \left(\sqrt{\frac{-Nr}{g}}, 0, \dots, 0 \right). \quad (12)$$

Here, we can choose the first component as the ordering direction without loss of generality. This solution is still invariant under $O(N-1)$ rotations that do not mix the first component. Thus, the spontaneous symmetry breaking of $O(N) \rightarrow O(N-1)$ occurs in the ordered state.

III. FLUCTUATIONS IN THE ORDERED STATE AT FINITE TEMPERATURE

A. Formal expression of transition point

At a finite temperature, thermal fluctuations may disrupt the ordered state at $T = 0$. To examine the thermal fluctuations under the flow, we consider the fluctuations $\sigma(t, \mathbf{x})$ and $\pi^\alpha(t, \mathbf{x})$ from the ordered state:

$$\phi^\alpha(t, \mathbf{x}) = (\sqrt{N}\bar{\phi}_R + \sigma(t, \mathbf{x}), \pi^\alpha(t, \mathbf{x})), \quad \alpha = 2, 3, \dots, N, \quad (13)$$

where $\bar{\phi}_R$ is the condensation including renormalization corrections. We note that π^α corresponds to the NG mode. From the leading-order calculation in the $1/N$ expansion, we can obtain the complete set of equations describing the condensation and fluctuations in the stationary state at $t \rightarrow \infty$

$$\bar{\phi}_R^2 = -\frac{1}{g} \left(r + g I_{\pi\pi} \right), \quad (14)$$

$$I_{\pi\pi} := \langle \pi(\mathbf{x})^2 \rangle = \int \frac{d\mathbf{k}}{(2\pi)^2} C_{\pi\pi}(\mathbf{k}), \quad (15)$$

$$C_{\pi\pi}(\mathbf{k}) = \frac{\Gamma T}{\Gamma \mathbf{k}^2 - (1/2)\mathbf{k} \cdot \mathcal{D} \cdot \nabla_{\mathbf{k}}}, \quad (16)$$

$$C_{\sigma\sigma}(\mathbf{k}) = \frac{\Gamma T}{\Gamma(\mathbf{k}^2 - 2r - 2g I_{\pi\pi}) - (1/2)\mathbf{k} \cdot \mathcal{D} \cdot \nabla_{\mathbf{k}}}, \quad (17)$$

where \mathbf{k} is the wavenumber and $\nabla_{\mathbf{k}} := \partial / \partial \mathbf{k}$. Here, we have introduced the static correlation $C_{XX}(\mathbf{k})$ by

$$\langle X(\mathbf{k})X(\mathbf{k}') \rangle = C_{XX}(\mathbf{k})(2\pi)^2 \delta(\mathbf{k} + \mathbf{k}'). \quad (18)$$

We abbreviate the superscript α of $\pi^\alpha(\mathbf{k})$ in $C_{\pi\pi}(\mathbf{k})$ because π^α are equivalent for all α owing to the $O(N-1)$ symmetry. The expressions (14)–(17) are valid for any S and A . The deviation is given in appendix A. Note that $I_{\pi\pi}$ gives the one-loop renormalization corrections to $\bar{\phi}_R^2$ and $C_{\sigma\sigma}(\mathbf{k})$. In particular, we have the renormalized "mass" of σ as

$$m_\sigma^2 = -2r - 2g I_{\pi\pi} \quad (19)$$

from the denominator of (17) in $\mathbf{k} \rightarrow \mathbf{0}$. In contrast, π^α is protected from mass renormalization because it is the NG mode. We note that the renormalization correction $I_{\pi\pi}$ vanishes at $T \rightarrow 0$, and then we recover the condensate (12) at $T = 0$.

The transition point between the ordered and disordered phases is determined by the stability of the ordered state. The ordered state is stable if the renormalized mass squared is non-negative $m_\sigma^2 \geq 0$, whereas it is unstable if the renormalized mass squared is negative $m_\sigma^2 < 0$. Then, from (19), we have the transition point r^* as

$$r^* = -gI_{\pi\pi}, \quad (20)$$

$$= -g \int \frac{d\mathbf{k}}{(2\pi)^2} C_{\pi\pi}(\mathbf{k}), \quad (21)$$

where we use (15) in the second equality. This equation provides the relationship between the transition point r^* and the static correlation $\pi(\mathbf{k})$ of the NG mode. The transition point r^* may diverge to $-\infty$ owing to the IR singularities of $C_{\pi\pi}(\mathbf{k})$. Because the ordered state is unstable for $r > r^*$, the negative divergence of r^* implies that the ordered state is not realized for any finite r . Consequently, it turns out that the realization of the ordered state can be identified by examining the IR divergence of the integral (21).

In fact, in the equilibrium case with $\mathcal{D} = 0$, $C_{\pi\pi}(\mathbf{k})$ is calculated as T/\mathbf{k}^2 from (16) and results in the logarithmic divergence of r^* in 2D:

$$r^* = -g \int_{2\pi/L}^{2\pi/a} \frac{d\mathbf{k}}{(2\pi)^2} \frac{T}{\mathbf{k}^2}, \quad (22)$$

$$= -\frac{gT}{2\pi} \log \frac{L}{a} \rightarrow -\infty. \quad (23)$$

This result is consistent with the HMW theorem (1).

B. Interplay between advection and diffusion

To evaluate the IR divergence of (21) for the various flow patterns, we derive the integral expression of $C_{\pi\pi}(\mathbf{k})$ from (16). To this end, we exponentiate the denominator of (16) by introducing the time integral

$$C_{\pi\pi}(\mathbf{k}) = \int_0^\infty dt U(t) \Gamma T, \quad (24)$$

$$U(t) := \exp \left[-t \left(\Gamma \mathbf{k}^2 - \frac{1}{2} \mathbf{k} \cdot \mathcal{D} \cdot \nabla_{\mathbf{k}} \right) \right], \quad (25)$$

As we will see in section V, $U(t)$ corresponds to the time-evolution operator of the NG mode. Then, we can regard the exponent of $U(t)$ as the Hamiltonian governing the time evolution:

$$H = \Gamma \mathbf{k}^2 - \frac{1}{2} \mathbf{k} \cdot \mathcal{D} \cdot \nabla_{\mathbf{k}}. \quad (26)$$

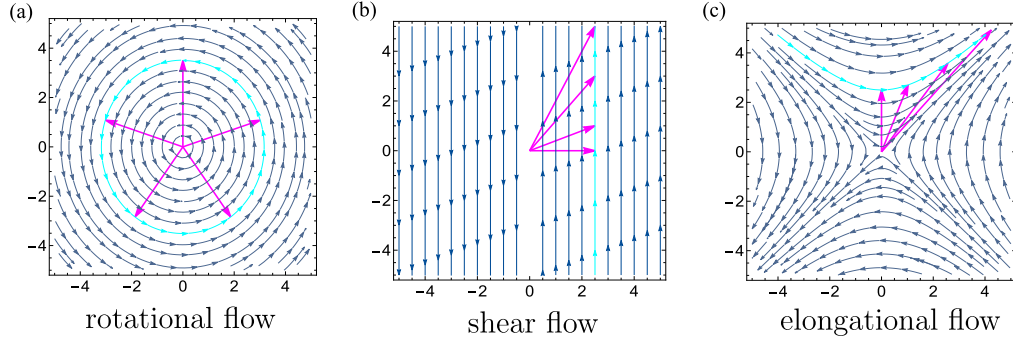


FIG. 2. Time evolution of the advected wavenumber $\mathbf{q}(t)$. The magenta arrows show $\mathbf{q}(t)$ at several times. The dark- and light-blue lines show the streamlines of $\tilde{\mathbf{v}}(\mathbf{k})$ and the line passing through $\mathbf{q}(0)$, respectively. (a): $\mathbf{q}(t)$ under the rotational flow with $S = 0.1$ and $A = 1.0$. (b): $\mathbf{q}(t)$ under the shear flow with $S = A = 0.2$. (c): $\mathbf{q}(t)$ under the elongational flow with $S = 1$ and $A = 0$.

This Hamiltonian consists of two parts:

$$H_I = \Gamma \mathbf{k}^2 \text{ and } H_0 = -\frac{1}{2}(\mathcal{D}^T \cdot \mathbf{k}) \cdot \nabla_{\mathbf{k}}. \quad (27)$$

The first part H_I describes diffusive relaxation, whereas the second part H_0 describes advective transport. The interplay between H_I and H_0 results in the rich behaviors of $U(t)$ or $C_{\pi\pi}(\mathbf{k})$. To decompose the roles played by diffusion and advection, we apply the interaction representation used in quantum mechanics and rewrite (25) as

$$U(t) = U_I(t)e^{tH_0}, \quad (28)$$

$$U_I(t) = \exp\left[-\Gamma \int_0^t d\tau \mathbf{q}(\tau)^2\right], \quad (29)$$

$$\mathbf{q}(\tau) := e^{\tau H_0} \mathbf{k} e^{-\tau H_0}. \quad (30)$$

Then, the correlation function becomes

$$C_{\pi\pi}(\mathbf{k}) = \Gamma T \int_0^\infty dt U_I(t) = \Gamma T \int_0^\infty dt \exp\left[-\Gamma \int_0^t d\tau \mathbf{q}(\tau)^2\right] \quad (31)$$

where e^{tH_0} of (28) becomes unity because it acts on the constant ΓT in (24). Here, we introduce the advected wavenumber $\mathbf{q}(\tau)$, which evolves with time according to only the advective transport H_0 . In the representation (31), the effects of advection are fully encapsulated in $\mathbf{q}(t)$, whereas the quadratic form of $\mathbf{q}(\tau)^2$ reflects the effects of diffusion.

C. Stability of the ordered state

From (21) and (31), we calculate the long-wavelength behaviors of $C_{\pi\pi}(\mathbf{k})$ and the stability of the ordered state at each flow. We first note that from (30), $\mathbf{q}(t)$ is the solution of the advection equation:

$$\frac{\partial}{\partial t}\mathbf{q}(t) = \tilde{\mathbf{v}}(\mathbf{k}) \cdot \nabla_{\mathbf{k}}\mathbf{q}(t), \quad (32)$$

$$\tilde{\mathbf{v}}(\mathbf{k}) = \frac{1}{2}\mathcal{D}^T \cdot \mathbf{k}, \quad (33)$$

with the initial condition $\mathbf{q}(0) = \mathbf{k}$. Then, $\mathbf{q}(t)$ evolves along the streamlines of $\tilde{\mathbf{v}}(\mathbf{k})$ without the diffusion. In Fig. 2, we plot the time evolution of $\mathbf{q}(t)$, which significantly depends on the flow pattern. In the long-time limit, we can calculate the asymptotic behaviors of $q^2(t)$ as

$$q_s^2(t) \sim t^2 k_x^2, \quad q_e^2(t) \sim e^{t\Omega_e} k_{\text{out}}^2, \quad q_r^2(t) \sim k^2. \quad (34)$$

where the subscripts s , e , and r denote the shear, elongational, and rotational flows, respectively. Here, $\Omega_e = \sqrt{S^2 - A^2}$ and k_{out} is the wavenumber along the outgoing direction of the elongational flow in Fig. 2-(b). See appendix B for details. Then, substituting (34) into (29) yields the dependence of $U_I(t)$ on the flow patterns

$$U_I^s(t) \sim e^{-\Gamma S^2 k_x^2 t^3}, \quad U_I^e(t) \sim e^{-\Gamma S^2 \Omega_e^{-1} k_{\text{out}}^2 e^{t\Omega_e}}, \quad U_I^r(t) \sim e^{-\Gamma k^2 t}. \quad (35)$$

By integrating (35) in time, we can derive the asymptotic expressions of $C_{\pi\pi}(\mathbf{k})$ from (31). We first consider the time integrals of $U_I^s(t)$ and $U_I^r(t)$. We extract the wavenumber dependences of the time integrals of $U_I^s(t)$ and $U_I^r(t)$ by changing the time variables as

$$\int_0^\infty dt U_I^s(t) \sim \int_0^\infty dt e^{-\Gamma S^2 k_x^2 t^3} = \frac{1}{k_x^{2/3}} \int_0^\infty d\tau_s e^{-\Gamma S^2 \tau_s^3}, \quad (36)$$

$$\int_0^\infty dt U_I^r(t) \sim \int_0^\infty dt e^{-\Gamma k^2 t} = \frac{1}{k^2} \int_0^\infty d\tau_r e^{-\Gamma \tau_r}, \quad (37)$$

where $\tau_s = k_x^{2/3} t$ and $\tau_r = k^2 t$. We note that the integral parts of the right-hand side do not depend on the wavenumber. Thus, we have the asymptotic behaviors

$$C_{\pi\pi}^s(\mathbf{k}) \sim \frac{1}{k_x^{2/3}}, \quad (38)$$

$$C_{\pi\pi}^r(\mathbf{k}) \sim \frac{1}{k^2}. \quad (39)$$

We next consider the time integral of $U_I^e(t)$. By introducing the time variable as

$$\tau_e = \Gamma S^2 \Omega_e^{-1} k_{\text{out}}^2 e^{t\Omega_e}, \quad (40)$$

we have

$$\int_0^\infty dt U_I^e(t) \sim \int_0^\infty dt \exp\left[-\Gamma S^2 \Omega_e^{-1} k_{\text{out}}^2 e^{t\Omega_e}\right] = \frac{1}{\Omega_e} \int_{\Gamma S^2 \Omega_e^{-1} k_{\text{out}}^2}^\infty \frac{e^{-\tau}}{\tau}, \quad (41)$$

$$= -\frac{1}{\Omega_e} \text{Ei}(-\Gamma S^2 \Omega_e^{-1} k_{\text{out}}^2), \quad (42)$$

where $\text{Ei}(x)$ is the exponential integral function

$$\text{Ei}(x) = -\int_{-x}^\infty d\tau \frac{e^{-\tau}}{\tau}. \quad (43)$$

The exponential integral function is represented as [65]

$$\text{Ei}(x) = \log x + \gamma - \text{Ein}(-x), \quad (44)$$

where γ is the Euler constant and $\text{Ein}(x)$ is the entire function. Because $\text{Ein}(x)$ is a regular function, the singularity of (C7) in the limit $k_{\text{out}} \rightarrow 0$ is given by

$$\int_0^\infty dt U_I^e(t) \sim \int_0^\infty dt \exp\left[-\Gamma S^2 \Omega_e^{-1} k_{\text{out}}^2 e^{t\Omega_e}\right], \quad (45)$$

$$\sim -\frac{1}{\Omega_e} \log k_{\text{out}}^2. \quad (46)$$

The resulting asymptotic forms of $C_{\pi\pi}(\mathbf{k})$ are summarized as

$$C_{\pi\pi}^s(\mathbf{k}) \sim \frac{1}{k_x^{2/3}}, \quad C_{\pi\pi}^e(\mathbf{k}) \sim -\log |k_{\text{out}}|, \quad C_{\pi\pi}^r(\mathbf{k}) \sim \frac{1}{k^2}. \quad (47)$$

The rotational flow does not change the asymptotic form of $C_{\pi\pi}(\mathbf{k})$ from that of equilibrium. Then, as shown in (23), the transition point r^* diverges to $-\infty$ and the ordered state does not appear for any finite r . We note that the rotational flow includes both purely rotational ($S = 0$) and elliptic ($S \neq 0$) flows. The elliptic flow drives the systems out of equilibrium and explicitly breaks a spatial rotational symmetry. Then, our result shows that the nonequilibrium conditions do not necessarily stabilize the LRO in 2D. In contrast, for the purely rotational flow, the absence of the ordered state is trivial because the system under this flow is equivalent to the equilibrium systems observed from rotating frames.

The shear and elongational flows significantly change the asymptotic behaviors of $C_{\pi\pi}(\mathbf{k})$. The divergent behaviors of $1/k_x^{2/3}$ and $-\log |k_{\text{out}}|$ are weaker than the equilibrium behavior

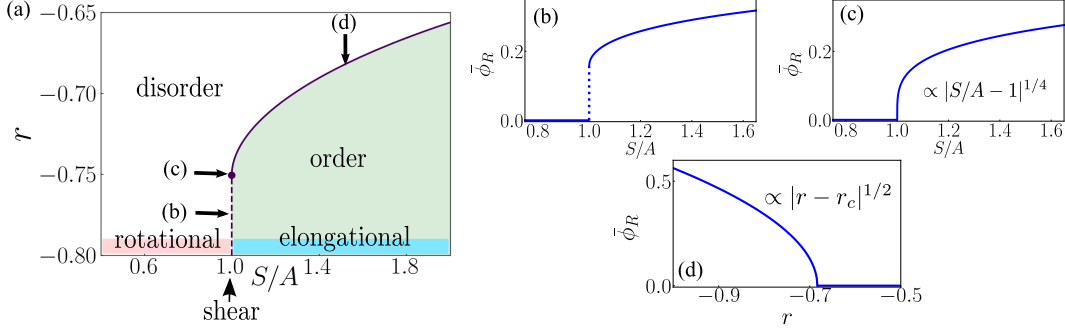


FIG. 3. (a): Phase diagram in $(r, S/A)$ space. (b)–(d): S/A or r dependence of the order parameter around the phase boundaries that are specified in (a). In (a), the phase boundary indicated by the dotted line is of the first order, whereas that indicated by the solid curve is of the second order. In all figures, we set the parameters to $g = \Gamma = T = A = 1$.

$1/k^2$, implying that the fluctuations are anomalously suppressed by the flows. We recall that as shown in (23), the IR divergence due to the $1/k^2$ behavior is marginal in 2D; the weaker divergences under the shear and elongational flows do not lead to the IR divergence of r^* . As a result, the LRO in 2D can stably exist for finite r . Therefore, the HWM theorem is violated under the shear and elongational flows. The results are summarized in Tab. I.

IV. PHASE DIAGRAM

We numerically calculate the transition point and draw the phase diagram. From (21) and (31), we obtain an explicit expression of the transition point

$$r^* = -gT \int \frac{d\mathbf{k}}{(2\pi)^2} \int_0^\infty dt \exp\left[-\Gamma \int_0^t d\tau q(\tau)^2\right]. \quad (48)$$

We perform numerical integration to obtain the phase boundary $r^*(S, A)$ as a function of S and A . See appendix D for the detailed procedure. In Fig. 3 (a), we present the phase diagram in $(r, S/A)$ space with $A = 1$. We note that the flow patterns can be controlled by changing the value of S/A . The phase transition occurs in the parameter range of the shear ($S/A = 1$) and elongational ($S/A > 1$) flows, whereas in the regime of rotational ($S/A < 1$) flow, the transition point r^* diverges to $-\infty$ and no ordered phase appears.

In Fig. 3 (b)–(d), we plot the onset behavior of the order parameter for different combinations of r and S/A . Three characteristic types of behavior are observed in these parameter

values. The first type presented in Fig. 3 (b) occurs when the flow pattern changes from rotational ($S/A < 1$) to elongational ($S/A > 1$) under a sufficiently small r [dotted line in Fig. 3 (a)]. In this case, the order parameter exhibits a discontinuous jump at $S/A = 1$, indicating that the phase transition is of the first order. As r increases, the jump width approaches 0 and a continuous phase transition appears at the endpoint [(c) in Fig. 3 (a)], which is the second type presented in Fig. 3 (c). The onset behavior at the endpoint is described by

$$\bar{\phi}_R \propto \left(\frac{S}{A} - 1 \right)^{1/4}. \quad (49)$$

Finally, the third type presented in Fig. 3 (d) occurs at the phase boundary where r decreases with the shear and elongational flows kept constant [solid curve in Fig. 3 (a)]. In this case, the order parameter behaves as

$$\bar{\phi}_R \propto |r - r^*|^{1/2}. \quad (50)$$

These critical exponents coincide with the mean-field values because the IR divergence is suppressed. See appendix E for the derivation of the exponents.

V. PHYSICAL MECHANISM UNDERLYING THE VIOLATION OF THE HWM THEOREM

We discuss the physical mechanism underlying our results on the basis of (24), which connects the static correlation of the NG mode to their dynamics. We show that the shear and elongational flows cause the superdiffusion of the NG mode, which decays faster than normal diffusion and leads to the LRO in 2D.

The time correlation function of the NG mode obeys the following equation of motion

$$\left[\frac{\partial}{\partial t} - \frac{1}{2} \mathbf{k} \cdot \mathcal{D} \cdot \nabla_{\mathbf{k}} + \Gamma \mathbf{k}^2 \right] D_{\pi\pi}(t, \mathbf{k}) = 0, \quad (51)$$

where $D_{\pi\pi}(t, \mathbf{k}) := \langle \pi^\beta(t, \mathbf{k}) \pi^\beta(0, -\mathbf{k}) \rangle / L^2$. The derivation is given in appendix F. We can write the formal solution using the time evolution operator $U(t)$ of (25) as

$$D_{\pi\pi}(t, \mathbf{k}) = U(t) D_{\pi\pi}(0, \mathbf{k}). \quad (52)$$

Therefore, (24) is interpreted as the formula that connects the static correlation of the NG mode with their dynamics. Because (24) remains valid even in equilibrium ($\mathbf{v} = 0$), it allows

us to study how the nonequilibrium dynamics changes the behavior of the static correlation of the NG mode.

We then examine the diffusion process of the NG mode described by $U(t)$. By rewriting (52) using (28), we obtain

$$D_{\pi\pi}(t, \mathbf{k}) = U_I(t) e^{tH_0} D_{\pi\pi}(0, \mathbf{k}), \quad (53)$$

$$= \exp\left[-\Gamma \int_0^t d\tau \mathbf{q}(\tau)^2\right] D_{\pi\pi}(t=0, \mathbf{q}(t)). \quad (54)$$

This equation indicates that $D_{\pi\pi}(t, \mathbf{k})$ exhibits the diffusion governed by $U_I(t)$, whereas e^{tH_0} only advects the wavenumber of the initial state.

We have obtained the long-time behaviors of $U_I(t)$ in (35). For the rotational flow, the time evolution operator behaves as $U_I^r(t) \sim e^{-\Gamma k^2 t}$, implying that the NG mode experiences the normal diffusion as in equilibrium. In contrast, for the shear and elongational flows, the evolution operators behave as $U_I^s(t) \sim e^{-\Gamma S^2 k_x^2 t^3}$ and $U_I^e(t) \sim e^{-\Gamma S^2 \Omega_e^{-1} k_{\text{out}}^2 e^{t\Omega_e}}$, respectively. These decays are faster than the normal diffusion and are called superdiffusion. Note that $U_I^s(t) \sim e^{-\Gamma S^2 k_x^2 t^3}$ corresponds to the sublinear dispersion $\omega \sim k_x^{2/3}$ of the NG mode under the shear flow [23].

Recall that the normal diffusion results in the marginal divergence of the transition point, as shown in (23) and (37). Superdiffusion, which decays faster than the normal diffusion, suppresses the marginal divergence of the fluctuations and stabilizes the LRO in 2D. We have shown in the latter part of section III C that the superdiffusion results in finite r^* . This is the physical mechanism underlying the violation of the HWM theorem in our model. The results are summarized in Tab. II

Note that whether superdiffusion occurs can be determined solely by examining the geometry of the streamlines associated with each type of flow. In the rotational flow [Fig. 2(a)], the streamlines form closed curves, whereas in the shear and elongational flows [Figs. 2(b) and (c)], they form open curves extending towards infinity. The occurrence of superdiffusion is

Type of advection	Streamline	Dynamics of NG mode	LRO in 2D
Rotational	closed curve	normal diffusion	No
Shear	infinitely outward	superdiffusion	Yes
Elongational	infinitely outward	superdiffusion	Yes

TABLE II. Relationship between dynamics of NG mode and LRO in 2D

crucially dependent on the streamline being open. See appendix G for a detailed discussion.

VI. CONCLUDING REMARKS

We have studied the $1 + 2$ dimensional $O(N)$ scalar model under different types of flow: shear, elongational, and rotational. We have demonstrated that the shear and elongational flows stabilize the LRO in 2D that is absent in equilibrium systems, according to the HMW theorem. The significant point of our analysis is to explicitly establish the connection (24) between the static correlations of the NG mode and their dynamics based on an interaction representation. In the interaction representation, the advective effect is encapsulated in the advected wavenumber $q(t)$, which evolves in time along the streamline of flows as shown in Fig. 2. We have shown that the interplay between the advection and diffusion causes superdiffusion and thereby stabilizes the LRO in 2D under the shear and elongational flows. In contrast, the rotational flow gives the normal diffusion as in equilibrium and does not stabilize the LRO in 2D. We have also numerically calculated the transition point and drawn the phase diagram. We have found that the order of the phase transition depends on r , as shown in Fig. 3.

Recently, it has been reported that in flocking hydrodynamics, the nonlinear interactions induced by the advective transport play a crucial role in stabilizing the LRO in 2D [9–12, 18–20]. In the flocking hydrodynamics, the advection arises from the self-propelled motions of active matter. This is different from our model, where the advection is induced by the external flow. However, both models share the common feature that the advective transport gives rise to the LRO in 2D that is absent in equilibrium systems. Therefore, it is interesting to establish the relationship between the self-advection in the active matter and the flow advection in our models. We leave it as our future work.

We note that fluctuations generally tend to be suppressed in the large- N limit and become larger at finite N . In some models such as the $SU(N)$ Thirring model, the NG mode is not included in the large- N limit and we have to include it manually for a correct analysis [66]. However, in the $O(N)$ model, (14) and (17) have the one-loop corrections of the NG mode even in the large- N limit. Then, we expect that the ordered state of our model will not be broken even at finite N . Indeed, the LRO under the shear flow at $N = 2$ has been established by the sophisticated numerical simulation [24]. In addition, the superdiffusion of the elongational

flow is much faster than the shear flow, whereas the rotational flow cannot stabilize even in the large- N limit. Therefore, our results will be qualitatively valid at finite N .

We finally remark on the possible realization of our results in experiments. We expect our setup to be implemented in the synchronization transition of chemical oscillation reactions [67, 68]. In the uniform oscillation of the synchronization transition, the $U(1)$ phase symmetry is spontaneously broken and it is possible to induce steady flows in a chemical reaction solution. In particular, the two-dimensional elongational flow has recently been realized in an experiment [69]. Thus, from the results presented in this paper, we expect that the uniform oscillation under the rotational flow will be disturbed as the system size increases, whereas it is sustained under the shear and elongational flows.

ACKNOWLEDGEMENTS

We are grateful to Keiji Saito and Yoshimasa Hidaka for valuable discussions. This work is supported by JSPS KAKENHI (Grant Numbers JP19H05791, JP21J00034, and JP22K13978). We also thank the Yukawa Institute for Theoretical Physics at Kyoto University and RIKEN iTHEMS. Discussions during the workshop (YITP-T-24-04) on “Advances in Fluctuating Hydrodynamics: Bridging the Micro and Macro Scales” were useful to complete this work.

Appendix A: Correlation functions in $1/N$ expansion

We derive (14), (16), and (17). For later convenience, we recast the equation of motion (5) into the form

$$\frac{\partial}{\partial t} \phi^a = -\Gamma \left[\chi_0^{-1} + \frac{g}{N} \sum_b (\phi^b)^2 \right] \phi^a + \eta^a, \quad (\text{A1})$$

$$\chi_0^{-1} = \mathbf{x} \cdot \frac{\mathcal{D}^T}{\Gamma} \cdot \nabla - \nabla^2 + r. \quad (\text{A2})$$

We consider the fluctuations $\sigma(t, \mathbf{x})$ and $\pi^\alpha(t, \mathbf{x})$ from $\bar{\phi}_R$ in the ordered state:

$$\phi^a(t, \mathbf{x}) = (\sqrt{N} \bar{\phi}_R + \sigma(t, \mathbf{x}), \pi^\alpha(t, \mathbf{x})), \quad (\text{A3})$$

where $\alpha = 2, 3, \dots, N$. Substituting (A3) into (A1), we obtain

$$\begin{aligned} & \left[\frac{1}{\Gamma} \frac{\partial}{\partial t} + \chi_0^{-1} + 3g\bar{\phi}_R^2 + \frac{g}{N} \left(\sum_{\alpha} (\pi^{\alpha})^2 + \sigma^2 \right) \right] \sigma \\ & + \sqrt{N}\bar{\phi}_R \left[r + g\bar{\phi}_R^2 + \frac{g}{N} \left(\sum_{\alpha} (\pi^{\alpha})^2 + 3\sigma^2 \right) \right] = \frac{\eta^1}{\Gamma}, \end{aligned} \quad (\text{A4})$$

$$\left[\frac{1}{\Gamma} \frac{\partial}{\partial t} + \chi_0^{-1} + g\bar{\phi}_R^2 + \frac{g}{N} \left(\sum_{\alpha} (\pi^{\alpha})^2 + \sigma^2 + 2\sqrt{N}\bar{\phi}_R\sigma \right) \right] \pi^{\beta} = \frac{\eta^{\beta}}{\Gamma}. \quad (\text{A5})$$

We calculate the correlation functions in $1/N$ expansion, and thus, counting N is important. We note that the π^{α} correlation yields the factor $N - 1$ as

$$\sum_{\alpha} \langle (\pi^{\alpha})^2 \rangle = (N - 1) \langle (\pi^{\beta})^2 \rangle, \quad (\text{A6})$$

where π^{β} is an arbitrary component and equivalent to the other components owing to the $O(N - 1)$ symmetry. In contrast, the number of σ is one, and thus, $\langle \sigma^2 \rangle$ does not yield the factor N .

Then, for the leading order calculation, we can replace the nonlinear term with

$$\frac{1}{N} \left(\sum_{\alpha} (\pi^{\alpha})^2 + \sigma^2 \right) \sim \langle (\pi^{\beta})^2 \rangle, \quad (\text{A7})$$

$$\equiv I_{\pi\pi}, \quad (\text{A8})$$

and obtain

$$\left[\frac{1}{\Gamma} \frac{\partial}{\partial t} + \chi_0^{-1} + 3g\bar{\phi}_R^2 + gI_{\pi\pi} \right] \sigma + \sqrt{N}\bar{\phi}_R \left[r + g \left(\bar{\phi}_R^2 + I_{\pi\pi} \right) \right] = \frac{\eta^1}{\Gamma}, \quad (\text{A9})$$

$$\left[\frac{1}{\Gamma} \frac{\partial}{\partial t} + \chi_0^{-1} + g \left(\bar{\phi}_R^2 + I_{\pi\pi} \right) \right] \pi^{\beta} = \frac{\eta^{\beta}}{\Gamma}, \quad (\text{A10})$$

where we have discarded the subleading terms in $1/N$.

We first derive (14) for $\bar{\phi}_R$. By taking the noise average of (A9), we obtain

$$\bar{\phi}_R \left[r + g \left(\bar{\phi}_R^2 + I_{\pi\pi} \right) \right] = 0. \quad (\text{A11})$$

Therefore, we obtain (14) as $\bar{\phi}_R \neq 0$. In addition, by using (14), (A9) and (A10) respectively become

$$\left[\frac{\partial}{\partial t} + \mathbf{x} \cdot \mathcal{D} \cdot \nabla - \Gamma \left(\nabla^2 - 2r - 2gI_{\pi\pi} \right) \right] \sigma(t, \mathbf{x}) = \eta^1(t, \mathbf{x}), \quad (\text{A12})$$

$$\left[\frac{\partial}{\partial t} + \mathbf{x} \cdot \mathcal{D} \cdot \nabla - \Gamma \nabla^2 \right] \pi^{\beta}(t, \mathbf{x}) = \eta^{\beta}(t, \mathbf{x}). \quad (\text{A13})$$

We perform the Fourier transform on the space

$$\left[\frac{\partial}{\partial t} - \mathbf{k} \cdot \mathcal{D} \cdot \nabla_{\mathbf{k}} + \Gamma \left(\mathbf{k}^2 + 2r + 2gI_{\pi\pi} \right) \right] \sigma(t, \mathbf{k}) = \eta^1(t, \mathbf{k}), \quad (\text{A14})$$

$$\left[\frac{\partial}{\partial t} - \mathbf{k} \cdot \mathcal{D} \cdot \nabla_{\mathbf{k}} + \Gamma \mathbf{k}^2 \right] \pi^\beta(t, \mathbf{k}) = \eta^\beta(t, \mathbf{k}). \quad (\text{A15})$$

By multiplying (A14) by $\sigma(t, \mathbf{k}')$ and taking the noise average, we obtain

$$\left[\frac{1}{2} \frac{\partial}{\partial t} - \frac{1}{2} \mathbf{k} \cdot \mathcal{D} \cdot \nabla_{\mathbf{k}} + \Gamma \left(\mathbf{k}^2 + 2r + 2gI_{\pi\pi} \right) \right] C_{\sigma\sigma}(\mathbf{k}, t) = T, \quad (\text{A16})$$

where we have introduced $C_{\sigma\sigma}(\mathbf{k}, t)$ in $\langle \sigma(\mathbf{k}, t) \sigma(\mathbf{k}', t) \rangle = C_{\sigma\sigma}(\mathbf{k}, t) \delta(\mathbf{k} + \mathbf{k}')$. We have also used $\langle \eta^1(t, \mathbf{k}) \sigma(t, -\mathbf{k}) \rangle = T$. We can drop the time derivative term for the steady state at $t \rightarrow \infty$ and obtain

$$C_{\sigma\sigma}(\mathbf{k}) = \frac{T}{-(1/2) \mathbf{k} \cdot \mathcal{D} \cdot \nabla_{\mathbf{k}} + \Gamma \left(\mathbf{k}^2 + 2r + 2g \right)}. \quad (\text{A17})$$

We also obtain $C_{\pi\pi}(\mathbf{k})$ (16) by repeating the similar calculation for (A15).

Appendix B: Detailed calculation of $q(t)$

From the definition (30), $q(t)$ is written as

$$\mathbf{q}(t) = \mathcal{M}(t) \mathbf{k}, \quad (\text{B1})$$

$$\mathcal{M}(t) = \exp \left[\frac{t}{2} \mathcal{D}^T \right], \quad (\text{B2})$$

where the superscript T denotes the transpose of a matrix. The time dependence of $q(t)$ is determined by the matrix $\mathcal{M}(t)$.

To calculate $\mathcal{M}(t)$, we consider the eigenvalue λ_\pm and the eigenvector e_\pm of \mathcal{D}^T , which are respectively given by

$$\lambda_\pm = \pm \sqrt{S^2 - A^2}, \quad (\text{B3})$$

$$e_\pm = \frac{1}{\sqrt{2S}} \begin{pmatrix} \sqrt{S-A} \\ \pm \sqrt{S+A} \end{pmatrix}. \quad (\text{B4})$$

The eigenvalue λ_\pm is real for the elongational flow ($S > A$) and purely imaginary for the rotational flow ($A > S$). For the shear flow, the eigenvalue is zero and degenerate. From the

eigenvectors, we obtain the diagonalizing matrix for $S \neq A$,

$$P = \frac{1}{\sqrt{2S}} \begin{pmatrix} \sqrt{S-A} & \sqrt{S-A} \\ \sqrt{S+A} & -\sqrt{S+A} \end{pmatrix}. \quad (\text{B5})$$

We then calculate $\mathcal{M}(t)$ as follows:

$$\exp\left(\frac{t}{2}\mathcal{D}^T\right) = PP^{-1} \exp\left(\frac{t}{2}\mathcal{D}^T\right) PP^{-1}, \quad (\text{B6})$$

$$= P \begin{pmatrix} e^{t\lambda_+/2} & 0 \\ 0 & e^{t\lambda_-/2} \end{pmatrix} P^{-1}, \quad (\text{B7})$$

$$= \begin{pmatrix} \cosh(t\lambda_+/2) & \frac{S-A}{\lambda_+} \sinh(t\lambda_+/2) \\ \frac{S+A}{\lambda_+} \sinh(t\lambda_+/2) & \cosh(t\lambda_+/2) \end{pmatrix}, \quad (\text{B8})$$

where we have used $\lambda_+ = -\lambda_-$. Therefore, for the elongational flow $S > A$, we obtain

$$\mathcal{M}_e(t) = \begin{pmatrix} \cosh(t\Omega_e/2) & \frac{S-A}{\Omega_e} \sinh(t\Omega_e/2) \\ \frac{S+A}{\Omega_e} \sinh(t\Omega_e/2) & \cosh(t\Omega_e/2) \end{pmatrix}, \quad (\text{B9})$$

where we have introduced $\Omega_e = \lambda_+$. For the rotational flow $A > S$, Ω_e becomes $i\Omega_r = i\sqrt{A^2 - S^2}$ and hyperbolic functions also become trigonometric functions. Then, we obtain

$$\mathcal{M}_r(t) = \begin{pmatrix} \cos(t\Omega_r/2) & \frac{S-A}{\Omega_r} \sin(t\Omega_r/2) \\ \frac{S+A}{\Omega_r} \sin(t\Omega_r/2) & \cos(t\Omega_r/2) \end{pmatrix}. \quad (\text{B10})$$

For the shear flow $A = S$, Ω_e becomes zero and \mathcal{M}_e become

$$\mathcal{M}_s(t) = \begin{pmatrix} 1 & 0 \\ tS & 1 \end{pmatrix}. \quad (\text{B11})$$

Therefore, the square of $\mathbf{q}_i(t) = \mathcal{M}_i(t)\mathbf{k}$ is calculated as

$$\mathbf{q}_i^2(t) = \mathbf{k}^2 + \mathbf{k}^T \cdot \mathcal{F}_i(t) \cdot \mathbf{k}, \quad (\text{B12})$$

$$\mathcal{F}_s(t) = \begin{pmatrix} t^2 S^2 & tS \\ tS & 0 \end{pmatrix}, \quad (\text{B13})$$

$$\mathcal{F}_e(t) = \begin{pmatrix} \frac{2A}{S-A} \sinh^2(t\Omega_e/2) & \frac{2S}{\Omega_e} \sinh(\Omega_e t/2) \cosh(\Omega_e t/2) \\ \frac{2S}{\Omega_e} \sinh(\Omega_e t/2) \cosh(\Omega_e t/2) & -\frac{2A}{S+A} \sinh^2(t\Omega_e/2) \end{pmatrix}, \quad (\text{B14})$$

$$\mathcal{F}_r(t) = \begin{pmatrix} \frac{2S}{A-S} \sin^2(t\Omega_r/2) & \frac{2S}{\Omega_r} \sin(\Omega_r t/2) \cos(\Omega_r t/2) \\ \frac{2S}{\Omega_r} \sin(\Omega_r t/2) \cos(\Omega_r t/2) & -\frac{2S}{A+S} \sin^2(t\Omega_r/2) \end{pmatrix}. \quad (\text{B15})$$

Furthermore, in the long-time limit, we obtain

$$\mathbf{q}_s^2(t) \sim t^2 S^2 k_x^2, \quad (\text{B16})$$

$$\mathbf{q}_e^2(t) \sim \frac{1}{2} e^{t\Omega_e} \begin{pmatrix} k_x & k_y \end{pmatrix} \begin{pmatrix} S/(S-A) & S/\Omega_e \\ S/\Omega_e & S/(S+A) \end{pmatrix} \begin{pmatrix} k_x \\ k_y \end{pmatrix} \quad (\text{B17})$$

$$= e^{t\Omega_e} \begin{pmatrix} k_{\text{out}} & k_{\text{in}} \end{pmatrix} \begin{pmatrix} S^2/\Omega_e^2 & 0 \\ 0 & 0 \end{pmatrix} \begin{pmatrix} k_{\text{out}} \\ k_{\text{in}} \end{pmatrix}, \quad (\text{B18})$$

where we have diagonalized the matrix part of $\mathbf{q}_e^2(t)$ in the last line. We also introduce k_{out} and k_{in} as

$$\begin{pmatrix} k_{\text{out}} \\ k_{\text{in}} \end{pmatrix} = \frac{1}{\sqrt{2S}} \begin{pmatrix} \sqrt{S+A} & \sqrt{S-A} \\ -\sqrt{S-A} & \sqrt{S+A} \end{pmatrix} \begin{pmatrix} k_x \\ k_y \end{pmatrix}, \quad (\text{B19})$$

$$(\text{B20})$$

which are the wavenumbers in the outgoing and incoming directions of the elongational flow, respectively. The long-time behavior of $\mathbf{q}_r^2(t)$ does not change because it oscillates in time.

Finally, we consider the time integral of $\mathbf{q}_i^2(t)$, which are calculated as

$$\int_0^t d\tau \mathbf{q}_s^2(\tau) \sim \frac{1}{3} t^3 S^2 k_x^2, \quad (\text{B21})$$

$$\int_0^t d\tau \mathbf{q}_e^2(\tau) \sim \frac{S^2}{\Omega_e} e^{t\Omega_e} k_{\text{out}}^2, \quad (\text{B22})$$

$$\int_0^t d\tau \mathbf{q}_r^2(\tau) \sim t \mathbf{k}^2. \quad (\text{B23})$$

We note that the term with $\mathcal{F}_r(t)$ does not contribute to the time integral of $\mathbf{q}_r^2(t)$ in the long-time limit.

Appendix C: Derivation of (47)

We first derive $C_{\pi\pi}^s(\mathbf{k})$ and $C_{\pi\pi}^r(\mathbf{k})$ of (47) from U_I^s and U_I^r of (35), respectively. By changing the time variables as

$$\tau_s = k_x^{2/3} t, \quad (\text{C1})$$

$$\tau_r = k^2 t, \quad (\text{C2})$$

we can extract the wavenumber dependences of the time integrals of U_I^s and U_I^r

$$\int_0^\infty dt e^{-\Gamma S^2 k_x^2 t^3} = \frac{1}{k_x^{2/3}} \int_0^\infty d\tau_s e^{-\Gamma S^2 \tau_s^3}, \quad (C3)$$

$$\int_0^\infty dt e^{-\Gamma k^2 t} = \frac{1}{k^2} \int_0^\infty d\tau_r e^{-\Gamma \tau_r}, \quad (C4)$$

respectively. We note that the integral parts of the r.h.s do not depend on the wavenumber. Then, we obtain $C_{\pi\pi}^s(\mathbf{k})$ and $C_{\pi\pi}^r(\mathbf{k})$ of (35).

We next consider the time integral of $U_I^e(t)$. By changing the time variable as

$$\tau_e = \Gamma S^2 \Omega_e^{-1} k_{\text{out}}^2 e^{t\Omega_e}, \quad (C5)$$

we have

$$\int_0^\infty dt \exp\left[-\Gamma S^2 \Omega_e^{-1} k_{\text{out}}^2 e^{t\Omega_e}\right] = \frac{1}{\Omega_e} \int_{\Gamma S^2 \Omega_e^{-1} k_{\text{out}}^2}^\infty \frac{e^{-\tau}}{\tau}, \quad (C6)$$

$$= -\frac{1}{\Omega_e} \text{Ei}(-\Gamma S^2 \Omega_e^{-1} k_{\text{out}}^2), \quad (C7)$$

where Ei is the exponential integral function

$$\text{Ei}(x) = -\int_{-x}^\infty d\tau \frac{e^{-\tau}}{\tau}. \quad (C8)$$

The exponential integral function is represented as [65]

$$\text{Ei}(x) = \log x + \gamma - \text{Ein}(-x), \quad (C9)$$

where γ is the Euler constant and $\text{Ein}(x)$ is the entire function. Because $\text{Ein}(x)$ is the regular function, the singularity of (C7) in the limit $k_{\text{out}} \rightarrow 0$ is given by

$$\int_0^\infty dt U_I^e(t) = \int_0^\infty dt \exp\left[-\Gamma S^2 \Omega_e^{-1} k_{\text{out}}^2 e^{t\Omega_e}\right], \quad (C10)$$

$$\sim -\frac{1}{\Omega_e} \log k_{\text{out}}^2. \quad (C11)$$

Therefore, we arrive at $C_{\pi\pi}^e(\mathbf{k})$ of (47).

Appendix D: Procedure for drawing phase diagram

To draw the phase diagram, we calculate the transition point r^* without using the asymptotic behaviors in $t \rightarrow \infty$. From (21), (31), and (B1), we write the transition point $r^* = -gC_{\pi\pi}$

as

$$r^* = -\frac{gT}{4\pi^2} \int d\mathbf{k} \int_0^\infty ds \exp\left[-\mathbf{k}^T \cdot \Gamma \int_0^s d\tau \mathcal{M}_i^T \mathcal{M}_i \cdot \mathbf{k}\right]. \quad (\text{D1})$$

We note that apart from the IR divergence, $C_{\pi\pi}$ shows the UV divergence, which originates from $|\mathbf{k}| \rightarrow \infty$. The UV divergence exists even in three-dimensional equilibrium systems and is irrelevant to our purpose. To regulate it, we introduce $e^{-\epsilon \mathbf{k}^2}$ with the infinitesimally small parameter ϵ as

$$r^* = -gT \int \frac{d\mathbf{k}}{(2\pi)^2} \int_0^\infty ds \exp\left[-\mathbf{k}^T \cdot \Gamma \left(\int_0^s d\tau \mathcal{M}_i^T \mathcal{M}_i + \epsilon \mathcal{J}\right) \cdot \mathbf{k}\right], \quad (\text{D2})$$

where \mathcal{J} is the 2×2 unit matrix. By changing the order of the \mathbf{k} and s integrals, we perform the Gaussian integral for \mathbf{k} and obtain

$$r^* = -\frac{gT}{4\pi\Gamma} \int_0^\infty dt F_i(t), \quad (\text{D3})$$

$$F_i(t) \equiv \det\left(\int_0^t d\tau \mathcal{M}_i^T \mathcal{M}_i + \epsilon \mathcal{J}\right)^{-1/2}. \quad (\text{D4})$$

From (B9)–(B11), $F_i(t)$ are calculated as

$$F_r(t) = \left[\frac{2S^2(\cos(\Omega_r t) - 1) + \Omega_r^2 A^2 t^2}{\Omega_r^4} + 2\epsilon \left(t + \frac{tS^2}{\Omega_r^2} - \frac{S^2 \sin(\Omega_r t)}{\Omega_r^3} \right) \right]^{-1/2}, \quad (\text{D5})$$

$$F_e(t) = \left[\frac{2S^2(\cosh(\Omega_e t) - 1) - \Omega_e^2 A^2 s^2}{\Omega_e^4} + 2\epsilon \left(t - \frac{tS^2}{\Omega_e^2} + \frac{S^2 \sinh(\Omega_e t)}{\Omega_e^3} \right) \right]^{-1/2}, \quad (\text{D6})$$

$$F_s(t) = \left[\frac{1}{12} S^2 t^4 + s^2 + \epsilon \left(2t + \frac{1}{3} S^2 t^3 \right) \right]^{-1/2}. \quad (\text{D7})$$

We obtain r^* numerically by performing the t integral of $F_i(t)$. The resulting phase diagram is given in Fig. 3. We have set the parameters as $g = \Gamma = T = 1$ and $\epsilon = 10^{-3}$.

We also argue the UV divergence, which occurs in $\epsilon \rightarrow 0$. The leading term of $F_i(t)$ in the limit $t \rightarrow 0$ and the integral of that are calculated as

$$F_i(t) \propto \frac{1}{\sqrt{2\epsilon t}}, \quad (\text{D8})$$

$$\int_0^{\Lambda_0} dt F_i(t) \propto \sqrt{\frac{\Lambda_0}{2\epsilon}}, \quad (\text{D9})$$

where Λ_0 is the upper limit for the asymptotic behavior of $F_i(t)$. This behavior is common among the three flows. The integral diverges in the limit $\epsilon \rightarrow 0$, and thus, it is the UV divergence that we have regulated. Consequently, the UV divergence appears from the short-time behavior.

Appendix E: Derivation of critical exponents

We derive the scaling behavior $\bar{\phi}_R \sim \delta^{1/4}$ with $\delta \equiv S/A - 1$ in (49). From (14), (21), and (D3), we see that the dependence of $\bar{\phi}_R$ on S and A originates from the integral of $F_i(t)$.

The asymptotic behavior of $F_e(t)$ in $t \rightarrow \infty$ and its integral are respectively calculated as

$$F_e(s) = \frac{\Omega_e^2}{\sqrt{2S}} e^{-s\Omega_e/2}, \quad (\text{E1})$$

$$\int_{\Lambda_1}^{\infty} ds F_e(s) = \frac{\sqrt{2}\Omega_e}{S} e^{\Lambda_1\Omega_e/2}, \quad (\text{E2})$$

where Λ_1 is the cutoff for the asymptotic behavior. By expanding the integral in δ , we obtain the following in the leading order:

$$\int_{\Lambda_1}^{\infty} ds F_e(s) = \frac{\sqrt{2}}{S} \delta^{1/2}. \quad (\text{E3})$$

Therefore, we have $\bar{\phi}_R^2 \sim \delta^{1/2}$ and thus obtain the scaling behavior in (49).

We next derive the scaling behavior of (50). From (14) and (21), we obtain

$$\bar{\phi}_R = \frac{1}{g^{1/2}} (r - r^*)^{1/2}. \quad (\text{E4})$$

This is (50).

Appendix F: Time-evolution operator and interaction representation

We consider the time-correlation function $D_{\pi\pi}(t, \mathbf{k})$ defined by

$$D_{\pi\pi}(t, \mathbf{k}) := \langle \pi^\beta(t, \mathbf{k}) \pi^\beta(0, -\mathbf{k}) \rangle / L^2. \quad (\text{F1})$$

By multiplying (A15) by $\pi^\beta(0, -\mathbf{k})$ and taking the noise average, we obtain

$$\left[\frac{\partial}{\partial t} - \frac{1}{2} \mathbf{k} \cdot \mathcal{D} \cdot \nabla_{\mathbf{k}} + \Gamma \mathbf{k}^2 \right] D_{\pi\pi}(t, \mathbf{k}) = 0. \quad (\text{F2})$$

The solution is written as

$$D_{\pi\pi}(t, \mathbf{k}) = \exp \left[\frac{1}{2} t \mathbf{k} \cdot \mathcal{D} \cdot \nabla_{\mathbf{k}} - t \Gamma \mathbf{k}^2 \right] D_{\pi\pi}(t=0, \mathbf{k}). \quad (\text{F3})$$

We may regard the exponential part as the time-evolution operator $U(t)$ or the Green function with the Hamiltonians H_0 and H_I :

$$U(t) = \exp\left[\frac{1}{2}t\mathbf{k} \cdot \mathcal{D} \cdot \nabla_{\mathbf{k}} - t\Gamma\mathbf{k}^2\right], \quad (\text{F4})$$

$$\equiv \exp\left[tH_0 + tH_I\right], \quad (\text{F5})$$

$$H_0 = \mathbf{k} \cdot \mathcal{D} \cdot \nabla_{\mathbf{k}}/2, \quad (\text{F6})$$

$$H_I = -\Gamma\mathbf{k}^2. \quad (\text{F7})$$

To discuss the role of advection, we decompose the time evolution into those by the diffusion H_0 and the advection H_I as follows:

$$U_I(t) = e^{tH_I+tH_0}e^{-tH_0}. \quad (\text{F8})$$

$U_I(t)$ corresponds to the time-evolution operator in the interaction representation based on the reference frame of H_0 . The time derivative of $U_I(t)$ is calculated as follows:

$$\frac{\partial U_I(t)}{\partial t} = e^{tH_I+tH_0}\left(H_I + H_0 - H_0\right)e^{-tH_0}, \quad (\text{F9})$$

$$= e^{tH_I+tH_0}e^{-tH_0}\left(e^{tH_0}H_Ie^{-tH_0}\right), \quad (\text{F10})$$

$$= U_I(t)H_I(t), \quad (\text{F11})$$

where we have introduced $H_I(t) = e^{tH_0}H_Ie^{-tH_0}$. We note that the order of $U_I(t)$ and $H_I(t)$ on the r.h.s. is opposite to that in usual quantum mechanics. The formal solution is given by

$$U_I(t) = \tilde{\mathcal{T}} \exp\left[\int_0^t d\tau H_I(\tau)\right], \quad (\text{F12})$$

where $\tilde{\mathcal{T}}$ is the anti-time-ordered product:

$$\tilde{\mathcal{T}}\left[H_I(t_1)H_I(t_2)\right] = \begin{cases} H_I(t_1)H_I(t_2) & \text{for } t_1 < t_2, \\ H_I(t_2)H_I(t_1) & \text{for } t_1 > t_2. \end{cases} \quad (\text{F13})$$

$H_I(t)$ is calculated as

$$H_I(t) = -\Gamma e^{tH_0}\mathbf{k}^2 e^{-tH_0}, \quad (\text{F14})$$

$$= -\Gamma q(t)^2. \quad (\text{F15})$$

Here, $\mathbf{q}(t) \equiv e^{tH_0} \mathbf{k} e^{-tH_0}$ is the advected wavenumber. Because $H_I(t)$ is not the operator in the wavenumber space, we can drop $\tilde{\mathcal{T}}$ in (F12). Combining (F8), (F12), and (F15), we obtain

$$e^{tH_I+tH_0} = \exp\left[-\Gamma \int_0^t d\tau \mathbf{q}(\tau)^2\right] e^{tH_0}. \quad (\text{F16})$$

Therefore, we arrive at

$$D_{\pi\pi}(t, \mathbf{k}) = \exp\left[-\Gamma \int_0^t d\tau \mathbf{q}(\tau)^2\right] D_{\pi\pi}(t=0, \mathbf{q}(\tau)). \quad (\text{F17})$$

We note that an arbitrary function of the wavenumber $f(\mathbf{k})$ operated by $e^{t\mathbf{k} \cdot \mathcal{D} \cdot \nabla_{\mathbf{k}}/2}$ is written as the function of the advected wavenumber

$$\exp\left[t\mathbf{k} \cdot \mathcal{D} \cdot \nabla_{\mathbf{k}}/2\right] f(\mathbf{k}) = f(\mathbf{q}(t)). \quad (\text{F18})$$

Consequently, from (F17), we see that the average fluctuation $\langle \pi(t, \mathbf{k}) \rangle$ diffuses with the advected wavenumber $\mathbf{q}(\tau)$.

Appendix G: Superdiffusion and geometry of streamlines

We demonstrate that whether the superdiffusion occurs is determined solely by the geometry of the streamlines without explicit calculations. The key distinction among the rotational, shear, and elongational flows lies in the geometry of the streamline; as shown in Figs. 2(a)–(c), it forms a closed curve in the rotational flow and extends towards infinity in the shear and elongational flows.

As explained in section V, the dynamics of the NG mode is described by the time evolution operator $U_I(t)$, which is given by (54). Then, the difference in the geometries of the streamlines is reflected in the dynamics of the NG mode through the functional form of $\mathbf{q}(t)$. Because the advected wavenumber $\mathbf{q}(t)$ is the solution of the advection equations (32) and (33), $\mathbf{q}^2(t)$ is expressed as the quadratic form of \mathbf{k} :

$$\mathbf{q}^2(t) = \mathbf{k}^2 + \mathbf{k}^T \cdot \mathcal{F}(t) \cdot \mathbf{k}, \quad (\text{G1})$$

where the first term represents the equilibrium part and $\mathcal{F}(t)$ is a 2×2 matrix determined by the streamline in the wavenumber space. The expression of $\mathcal{F}(t)$ determines the behavior of $U_I(t)$, as shown in (35). The concrete expressions of $\mathcal{F}(t)$ are given in (B13)–(B15).

We first discuss the cases of shear and elongational flows, where the streamline goes towards infinity as shown in Figs. 2(b) and (c). The outgoing streamlines mean $q(t)^2 \rightarrow \infty$ at $t \rightarrow \infty$, which in turn implies $\mathcal{F}(t) \rightarrow \infty$ at $t \rightarrow \infty$. Then, the second term of (G1) is dominant and the asymptotic behavior is given by

$$q^2(t) \sim \mathcal{F}_{\text{out}}(t)k_{\text{out}}^2, \quad (\text{G2})$$

where k_{out} and $\mathcal{F}_{\text{out}}(t)$ are the components of \mathbf{k} and $\mathcal{F}(t)$ in the outgoing direction of the streamline, respectively. See (B16) and (B18) for the explicit expression of $q^2(t)$ in the long-time limit. By substituting (G2) into (54), we obtain

$$U_I(t) \sim e^{-\Gamma F(t)k_{\text{out}}^2} \quad (\text{G3})$$

with

$$F(t) := \int_0^t ds \mathcal{F}_{\text{out}}(s). \quad (\text{G4})$$

Because $\mathcal{F}_{\text{out}}(t) \rightarrow \infty$ at $t \rightarrow \infty$ due to the general feature of the outgoing streamline, its integral diverges faster than t . That is, we obtain

$$\lim_{t \rightarrow \infty} \frac{F(t)k_{\text{out}}^2}{tk^2} \rightarrow \infty, \quad (\text{G5})$$

which indicates the superdiffusion.

We next consider the case of rotational flow. In this case, in contrast to the shear and elongational flows, the streamline forms a closed curve such as that in Fig. 2(a). Because $q^2(t)$ and $\mathcal{F}(t)$ solely oscillate in time, the time integral of $\mathcal{F}(t)$ also oscillates. As a result, the first term of (G1) is dominant and we have

$$\int_0^t d\tau q^2(\tau) \sim tk^2. \quad (\text{G6})$$

Thus, we obtain the normal diffusion

$$U_I(t) \sim e^{-\Gamma k^2 t}. \quad (\text{G7})$$

[1] P. C. Hohenberg, Physical Review **158**, 383 (1967).

- [2] N. D. Mermin and H. Wagner, *Physical Review Letters* **17**, 1133 (1966).
- [3] N. D. Mermin, *Journal of Mathematical Physics* **8**, 1061 (2008).
- [4] N. D. Mermin, *Physical Review* **176**, 250 (1968).
- [5] D. R. Nelson and B. I. Halperin, *Physical Review B* **19**, 2457 (1979).
- [6] H. Tasaki, *Physical Review Letters* **125**, 220601 (2020).
- [7] H. Chaté, *Annual Review of Condensed Matter Physics* **11**, 189 (2020).
- [8] T. Vicsek, A. Czirók, E. Ben-Jacob, I. Cohen, I. and O. Shochet, *Physical Review Letters* **75**, 1226 (1995).
- [9] J. Toner and Y. Tu, *Physical Review Letters* **75**, 4326 (1995).
- [10] J. Toner and Y. Tu, *Physical Review E* **58**, 4828 (1998).
- [11] J. Toner, *Physical Review E* **86**, 031918 (2012).
- [12] J. Toner, *Physical Review Letters* **108**, 088102 (2012).
- [13] D. Nishiguchi, K. H. Nagai, H. Chaté, and M. Sano, *Physical Review E* **95**, 020601 (2017).
- [14] B. Mahault, F. Ginelli, and H. Chaté, *Physical Review Letters* **123**, 218001 (2019).
- [15] J. Iwasawa, D. Nishiguchi, and M. Sano, *Physical Review Research* **3**, 043104 (2021).
- [16] J. Codina, B. Mahault, H. Chaté, J. Dobnikar, I. Pagonabarraga, and X.-Q. Shi, *Physical Review Letters* **128**, 218001 (2022).
- [17] M. Besse, H. Chaté, and A. Solon, *Physical Review Letters* **129**, 268003 (2022).
- [18] H. Ikeda, *Arxiv:2403.02086* 10.48550/arXiv.2403.02086 (2024).
- [19] H. Chaté and A. Solon, *Arxiv:2403.03804* 10.48550/arXiv.2403.03804 (2024).
- [20] P. Jentsch and C. F. Lee, *Arxiv:2402.01316* 10.48550/arXiv.2402.01316 (2024).
- [21] P. G. De Gennes, *Molecular Crystals and Liquid Crystals* **34**, 91 (1976).
- [22] F. Corberi, G. Gonnella, E. Lippiello, and others, *Journal of Physics A: Mathematical and General* 10.1088/0305-4470/36/17/302 (2003).
- [23] Y. Minami, H. Nakano, and Y. Hidaka, *Physical Review Letters* **126**, 141601 (2021).
- [24] H. Nakano, Y. Minami, and S.-I. Sasa, *Physical Review Letters* **126**, 160604 (2021).
- [25] H. Nakano, Y. Minami, T. Haga, and S.-I. Sasa, *Arxiv:2107.13183* 10.48550/arXiv.2107.13183 (2021), *arXiv:2107.13183 [cond-mat.stat-mech]*.
- [26] L. Giomi, J. Toner, and N. Sarkar, *Physical Review E* **106**, 024701 (2022).
- [27] L. Giomi, J. Toner, and N. Sarkar, *Physical Review Letters* **129**, 067801 (2022).
- [28] D. Krommydas, L. N. Carenza, and L. Giomi, *Physical Review Letters* **130**, 098101 (2023).

- [29] K. E. Bassler and Z. Rácz, *Physical Review E* **52**, R9 (1995).
- [30] U. C. Täuber, V. K. Akkineni, and J. E. Santos, *Physical Review Letters* **88**, 045702 (2002).
- [31] M. D. Reichl, C. I. Del Genio, and K. E. Bassler, *Physical Review E* **82**, 040102 (2010).
- [32] L. P. Dadhichi, J. Kethapelli, R. Chajwa, S. Ramaswamy, and A. Maitra, *Physical Review E* **101**, 052601 (2020).
- [33] S. A. M. Loos, S. H. L. Klapp, and T. Martynec, *Physical Review Letters* **130**, 198301 (2023), arXiv:2206.10519 [cond-mat.stat-mech].
- [34] L. Galliano, M. E. Cates, and L. Berthier, *Physical Review Letters* **131**, 047101 (2023).
- [35] H. Ikeda and Y. Kuroda, arXiv:2304.14235 10.48550/arXiv.2304.14235 (2023).
- [36] R. Maire and A. Plati, Arxiv:2405.05621 10.48550/arXiv.2405.05621 (2024).
- [37] Y. Kuroda and K. Miyazaki, *Journal of Statistical Mechanics* **2023** (10), 103203.
- [38] Y. Kuroda, T. Kawasaki, and K. Miyazaki, Arxiv:2402.19192 10.48550/arXiv.2402.19192 (2024), arXiv:2402.19192 [cond-mat.soft].
- [39] B. Bergersen and Z. Rácz, *Physical Review Letters* **67**, 3047 (1991).
- [40] Y. Nambu and G. Jona-Lasinio, *Physical Review* **122**, 345 (1961).
- [41] J. Goldstone, *Il Nuovo Cimento* (1955-1965) **19**, 154 (1961).
- [42] J. Goldstone, A. Salam, and S. Weinberg, *Physical Review* **127**, 965 (1962).
- [43] Y. Minami and Y. Hidaka, *Physical Review E* **97**, 012130 (2018).
- [44] Y. Hidaka and Y. Minami, *Progress of Theoretical and Experimental Physics* **2020**, 033A01 (2020).
- [45] M. Hongo, S. Kim, T. Noumi, and A. Ota, *Physical Review D* **103**, 056020 (2021).
- [46] P. M. Chaikin, T. C. Lubensky, and T. A. Witten, *Principles of condensed matter physics*, Vol. 10 (Cambridge university press Cambridge, 1995).
- [47] H. Nishimori and G. Ortiz, *Elements of phase transitions and critical phenomena* (Oxford University Press, 2010).
- [48] P. L. Garrido, J. L. Lebowitz, C. Maes, and H. Spohn, *Physical Review A* **42**, 1954 (1990).
- [49] J. R. Dorfman, T. R. Kirkpatrick, and J. V. Sengers, *Annual Review of Physical Chemistry* **45**, 213 (1994).
- [50] J. M. O. de Zarate and J. V. Sengers, *Hydrodynamic fluctuations in fluids and fluid mixtures* (Elsevier, 2006).
- [51] H. Nakano and Y. Minami, *Physical Review Research* **4**, 023147 (2022).
- [52] H. Nakano and K. Adachi, *Physical Review Research* **6**, 013074 (2024).

- [53] S. Torquato, *Physics Reports* **745**, 1 (2018).
- [54] Q.-L. Lei and R. Ni, *Proceedings of the National Academy of Sciences* **116**, 22983 (2019).
- [55] H. Chaté, F. Ginelli, and R. Montagne, *Physical Review Letters* **96**, 180602 (2006).
- [56] V. Narayan, S. Ramaswamy, and N. Menon, *Science* **317**, 105 (2007).
- [57] H. P. Zhang, A. Be'er, E.-L. Florin, and H. L. Swinney, *Proceedings of the National Academy of Sciences* **107**, 13626 (2010).
- [58] A. Onuki and K. Kawasaki, *Annals of Physics* **121**, 456 (1979).
- [59] M. E. Cates and S. T. Milner, *Role of shear in the isotropic-to-lamellar transition* (1989).
- [60] S. Katz, J. L. Lebowitz, and H. Spohn, *Journal of Statistical Physics* **34**, 497 (1984).
- [61] K. Leung, *Physical Review Letters* **66**, 453 (1991).
- [62] E. L. Præstgaard, B. Schmittmann, and R. K. P. Zia, *The European Physical Journal B - Condensed Matter and Complex Systems* **18**, 675 (2000).
- [63] A. Onuki and K. Kawasaki, *Progress of Theoretical Physics* **63**, 122 (1980).
- [64] A. Onuki and K. Kawasaki, *Progress of Theoretical Physics Supplement* **69**, 146 (1980).
- [65] M. Abramowitz and I. A. Stegun, *Handbook of mathematical functions with formulas, graphs, and mathematical tables*, Vol. 55 (US Government printing office, 1968).
- [66] E. Witten, *Nuclear Physics B* **145**, 110 (1978).
- [67] Y. Kuramoto, *Chemical Oscillations, Waves, and Turbulence*, Dover Books on Chemistry Series (Dover Publications, 2003).
- [68] R. Toth, A. F. Taylor, and M. R. Tinsley, *The journal of physical chemistry B* **110**, 10170 (2006).
- [69] S. Varchanis, S. J. Haward, C. C. Hopkins, A. Syrakos, A. Q. Shen, Y. Dimakopoulos, and J. Tsamopoulos, *Proceedings of the National Academy of Sciences* **117**, 12611 (2020).